

Characteristics of Prototype Silicon Sensors for Run2b (I)

K. Hara and Y. Takei

University of Tsukuba, Tsukuba, Ibaraki, Japan

Abstract

We describe the characteristics of Hamamatsu silicon sensors prototyped for Run2b silicon detector. In the prototype program, 60 axial and 53 stereo sensors have been fabricated. The electrical and mechanical characteristics are superior in all the aspects and fulfill our specifications.

1. Introduction

The CDF collaboration is building a new silicon tracker system for Tevatron Collider Run2b, replacing the present L00 and SVXII detectors. The new silicon system will be a six-layer device located between 2.1 cm and 16 cm radius, consisting of ~2300 single sided silicon sensors. The new silicon detector is expected to become ready in 2005.

The specifications of silicon sensors are described in detail in CDF 6283. Table 1 summarizes the main specifications:

- Sensors should be operational up to 500V
- Full depletion voltage should be in the range from 120 to 250V
- Dead channel fraction should be less than 1%
- Sensors should be uniform in coupling capacitance, bias resistance, interstrip resistance, and other electrical properties

Table 1: Main sensor specifications

Specifications:	Inner Axial	Outer Axial/Outer Stereo
Wafer	Orientation: <100> Thickness: 320±15µm Warp: less than 130µm	
Full depletion voltage	120<Vdep<250V	
Leakage current	<50nA/cm ² at RT and at 500V	
Junction breakdown	>500V	
Implant width	7µm	8µm
Al width	1-3 µm overhanging metal	2-3 µm overhanging metal
Coupling capacitance	>12pF/cm	
Coupling capacitor breakdown	>100V	
Interstrip capacitance	<1.2pF/cm	
Polysilicon bias resistor	1.5±0.5 MΩ	
Defective strips	<1%	
Readout strip pitch	50 µm	75µm /80µm
Intermediate strip	yes	
Interstrip resistance	>1GΩ (after irradiation)	

3. Electrical Characteristics

We have evaluated the following electrical characteristics. The measurement procedures are described in detail in the accompanying note (CDF-6283). This note summarizes the results on the following items:

- (1) I-V curve: Total leakage current is measured as a function of bias voltage up to 1000V at a step of 10V.
- (2) Stability of I-V curve: I-V curves are measured every 30 min at least for 10 times. The bias voltage between the I-V measurements is kept at 200 V.
- (3) C-V curve: Total capacitance is measured as a function of bias voltage. The curve is used to extract the full depletion voltage.
- (4) AC scan: Coupling capacitance, implant + bias resistance, and oxide punch-through at 100V are measured for each readout strip.
- (5) DC scan: The leak current of individual strip is measured for sensors with large total leakage. The bias is set above the micro-discharge onset voltage.
- (6) Interstrip isolation: The interstrip resistance is measured with applying voltages (-1 to +1V) to the neighboring intermediate DC pads and measuring the current emerging from the readout DC pad.
- (7) Interstrip capacitance: The capacitance between the neighboring AC pads is measured with other strips floating to the ground.
- (8) Long-term stability: The leakage current is read out periodically while keeping the bias voltage at 500V.

In addition to the above, diagnostic measurements were carried out to identify the problems. Examples of such diagnostic measurements are:

- (1) DC scan on intermediate strips: When micro-discharge was identified from I-V measurement, we measured the individual strip current for the strips reported “Leaky” by HPK, or performed the full DC scan. This includes the DC scan on intermediate strips. Note, otherwise intermediate strips are not tested in usual scans. We can safely ignore somewhat leaky intermediate strips as far as the total leakage current is manageable.
- (2) Visual inspection: When the implant strip is reported “Open” by HPK, we first look at AC scan data (the coupling capacitance and series resistance are smaller if implant is open), then the strip is carefully inspected under microscope. If there is no clear open found, we measure the resistance between the DC pad and the bias-ring (very large if the intermediate implant is open), and other characteristics. We always inspect carefully under microscope when any irregularities are recognized.

3.1 I-V curves

Figures 1a and 1b show I-V curves of 60 axial and 53 stereo sensors. Most of the sensors do not show significant micro-discharge up to 1000V we measured. Exceptions are #010 and #048 stereo sensors, which showed micro-discharge at voltages above 300V-450V. As described in 3.5, single leaky strip contributes to the micro-discharge for both sensors. The I-V curve of these sensors became moderate by keeping the bias, as described in 3.2. We set our leakage current requirement to be less than 2 μA at 500V. This limit ensures that no single readout strip has a significant leakage current exceeding $\sim 1\mu\text{A}$. Actually, ISL sensors, which were double sided, had an average leakage current roughly one order more than the present sensors, and substantial

fraction had strip leakage current close to even a relaxed specification. The limit was set so that the noise performance is not degraded.

All the sensors fulfill our specification (S010 stereo is just on the boundary). Since the fraction of such micro-discharge sensors is small, two out of 113, we should avoid using such sensors as far as the production delivery goes as scheduled.

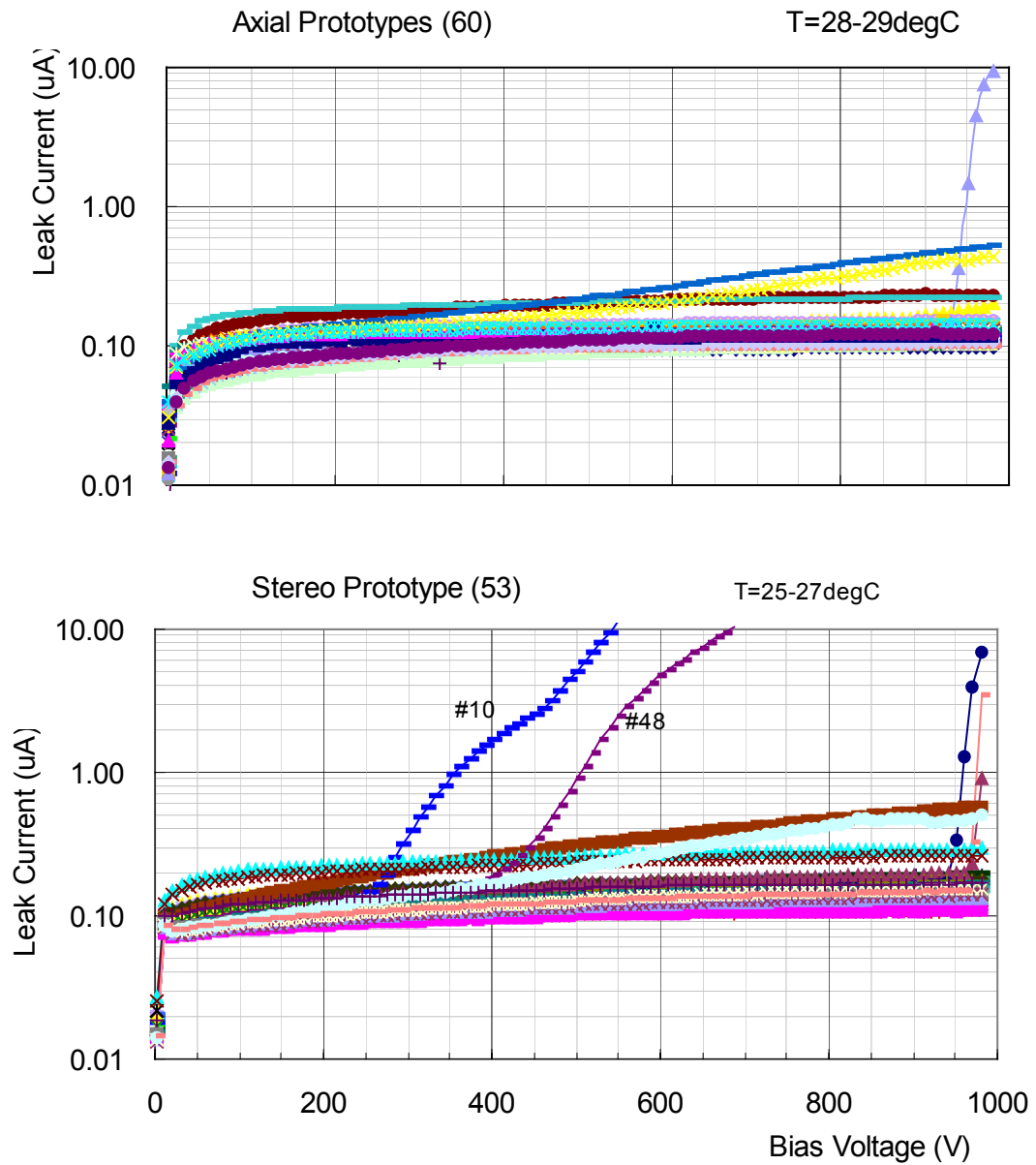


Fig. 1a (top) I-V curves of 60 axial sensors.

Fig. 1b (above) I-V curves of 53 stereo sensors.

3.2 Stability of I-V curves

The I-V measurement was repeated 20-30 times (10 times for some sensors) for sampled sensors. All the sensors which showed micro-discharges were tested. Between the I-V measurements, the sensors are biased to 200V and kept for 30 minutes. Figure 2a overlays I-V curves measured for a typical sensor, stereo #045. The curves are consistent and stable although the initial I-V tends to be somewhat different. This may be attributed to that the sensor surface condition has stabilized in time between.

Among the 7 axial sensors we measured, 6 sensors showed similar to the figure. This statistics includes one sensor measured by Purdue Group.

One sensor (axial A032: see Fig. 2b) showed initially good I-V. The I-V curves became in chaos after 7hr and the sensor drew a large current at 800V after 10 hr. We investigated the cause with an IR camera and found a deep trace of discharge on the bias ring. We suspect that a discharge occurred between the bias-ring (which is DC connected to a p+ implant underneath) and the substrate probably via defect in the wafer. The I-V of this sensor has not recovered indicating creation of permanent junction breakdown.

For stereo sensors, we measured I-V stability for 10 sensors. Sensor S010 (see Fig. 2c), which showed micro-discharge in the

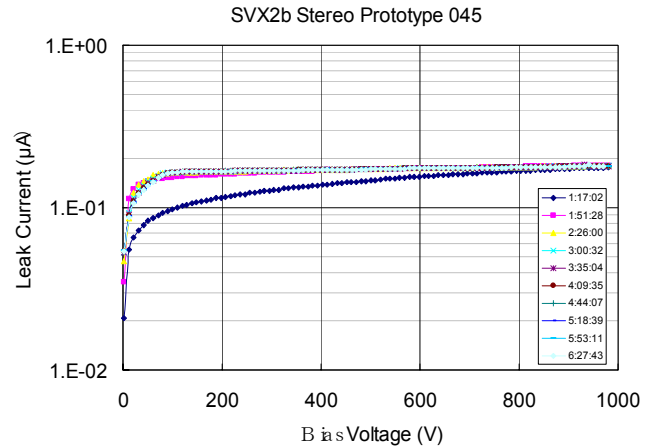


Fig. 2a Typical I-V stability of sensor S045 (stereo).

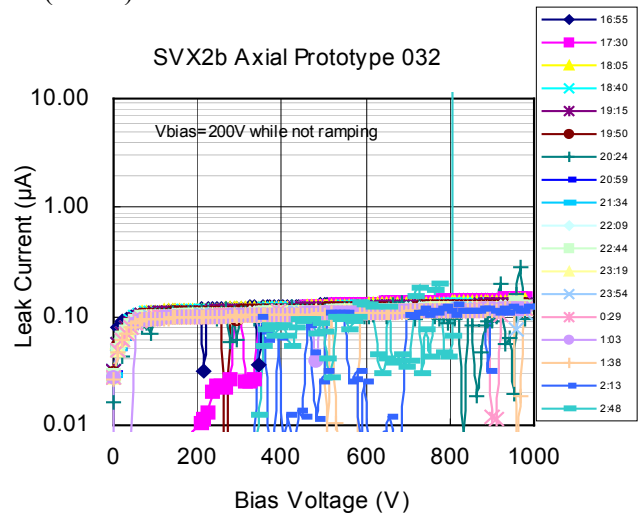


Fig. 2b Faulty I-V stability of sensor A032 (axial).

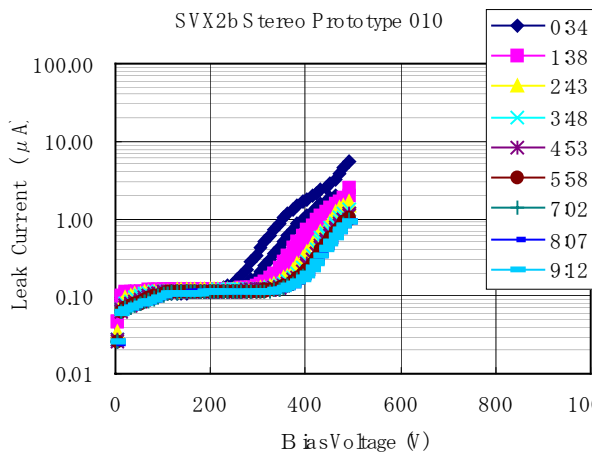


Fig. 2c I-V stability of sensor S010 (stereo).

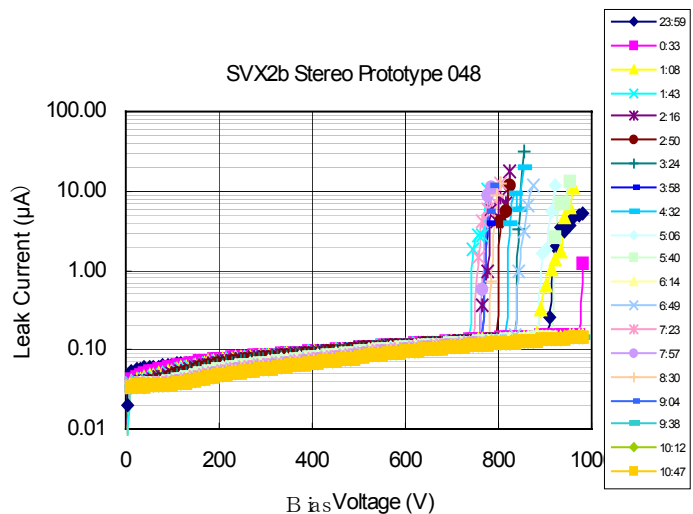


Fig. 2d I-V stability of sensor S048 (stereo).

initial I-V, improved the I-V curve gradually. The micro-discharge onset voltage of Sensor #048 (see Fig. 2d) was fluctuating around 800V. The I-V became flat to 1000V in the last three measurements. Note that the initial I-V is already better than the one shown in Fig. 1b because the sensor was biased for other test before this stability test. The rest of eight sensors showed stable I-V curves up to 1000V.

3.3 C-V curves

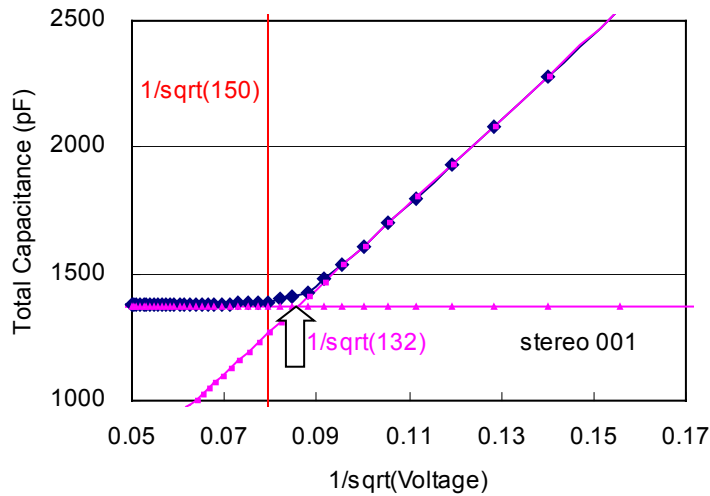


Fig. 3a C-V curve and evaluation of “the full depletion voltage”. HPK determines (see text) it to be 150V, whereas we obtain 132V for this sensor, stereo #001.

The C-V curves are measured for 19 axial and 53 stereo sensors at an LCR frequency of 400 Hz. We extract the full depletion voltage as the intercept of two straight lines in a $C-V^{1/2}$ plot (see Fig. 3a). HPK measures C-V at a voltage step of 10V. The data is used to evaluate the “full depletion voltage”, which is defined to be the lowest voltage where the increase of $1/C^2$ is found to be less than 2%. There is a tendency that HPK gives somewhat larger voltage, as can be seen in Fig. 3b. The distributions of Tsukuba data (axial and stereo separately) and of HPK are given in Fig. 3c. The spread of the distributions are similar, indicating that the full depletion voltages are extracted consistently apart from the

absolute value. As a matter of fact, the value 2% is an arbitral choice so that no fitting is necessarily performed. For a choice of 4%, the agreement between the two should be improved. Three sensors have failed in the full depletion voltage specification, but all of them are more than 115V.

Purdue Group has performed C-V measurement for four other axial sensors. The fitted full depletion voltages are larger than HPK values by 18-27 V, consistent to the present result.

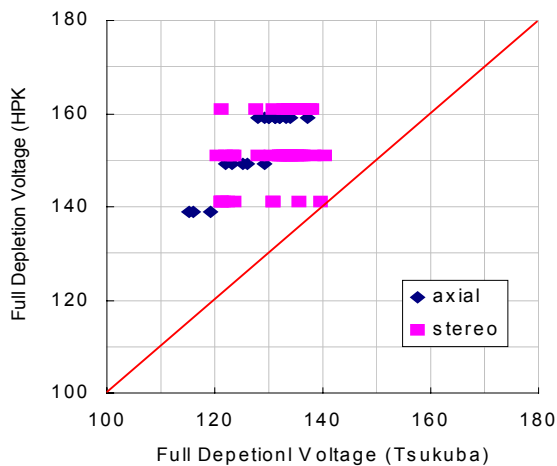


Fig. 3b Correlation of full depletion voltages defined by HPK and Tsukuba.

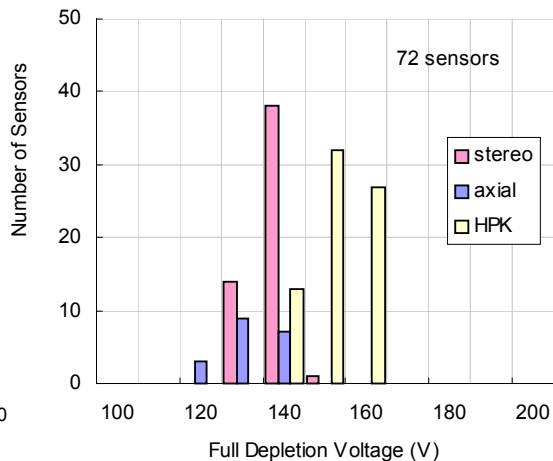


Fig. 3c Full depletion voltage distributions for axial and stereo sensors (Tsukuba) and for all (HPK).

3.4 AC scan

The strip integrity is intensively evaluated by AC scan where the measurement is performed in two steps. Firstly, capacitance and series resistance are measured by probing between the AC pad and bias-ring setting the LCR at Cs-Rs mode. Secondly, 100V is applied across for 1 second and then the leakage current through is measured. The capacitance represents the oxide coupling capacitance, and the resistance the sum of the bias resistance and implant electrode resistance. The latter contributes approximately 0.3-0.5 MΩ.

An example is shown in Fig. 4a, where the AC scan results are shown for stereo S068. Nominal values are about 120 pF (Ccp: coupling capacitance), 1.85 MΩ (R: series resistance), and less than 10 nA (Icp: leakage) for the strips with full length. As shown in the figure, coupling capacitance and R are smaller for shorter strips. Note that the 1st data point of R is small due to the frequency setting (1 kHz) is not at the optimum. Most part of the measured leakage Icp is actually through relays used in the measurement system. The leakage through genuine oxide layer is much smaller. If the oxide is completely punch-through, protection resistors in the system determine the leakage to ~9μA.

Some example results are shown in Fig.4b, where we found some defective strips. In total, AC scan is made for 18 axial sensors and 18 stereo sensors. The comparison of dead channels reported by HPK is described later.

Among the defective strips, there are a couple of cases where Icp is normal but R and Ccp are irregular. An example of such AC scans is given in Fig. 4c, where RD24 (-24 in the plot) has

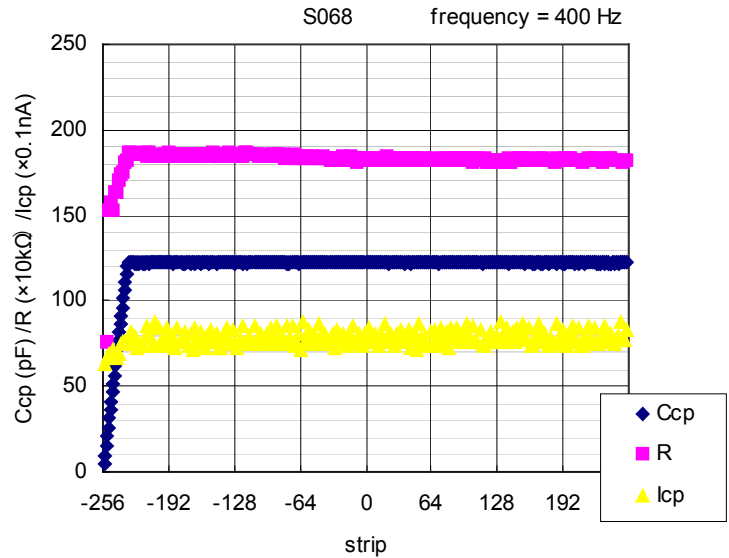


Fig. 4a Example of AC scan result (Stereo S068).

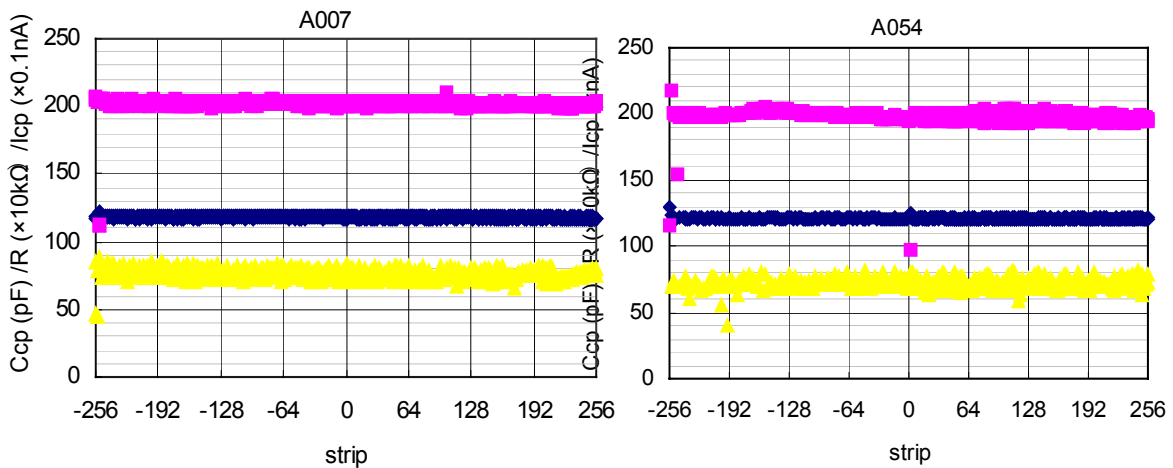
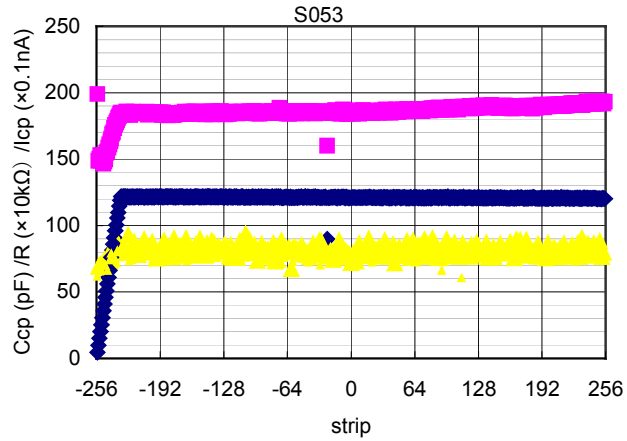


Fig. 4b AC scan result for (left) axial A007 and (right) axial A054

smaller R and Ccp values but Icp is normal. In this case, we found a clear break in the implant. HPK reports no defect with this strip. Later, we describe this discrepancy further in detail.

Fig. 4d AC scan for stereo S053. One strip (-24) shows irregular R and Ccp values. A clear break was found in this implant strip, while this defect was not recognized by HPK.



3.5 DC scan

DC scan was made only for leaky sensors. An example result for stereo sensor S010 is given in Fig. 5, where the total leakage current evolution during the measurement is also plotted. The bias is set to 400 V, above the micro-discharge onset voltage. The total leakage decreases as the measurement proceeds (scans from -256 to 256), as we have seen in I-V stability test. Since the total leakage current is about 0.1-0.2 μA for good sensors, the excess of this sensor is initially about 1 μA and finally 0.1 μA . The excess is totally explained by a single leaky strip, U225.

This strip is classified as dead (Leaky) by HPK. Another leaky sensor (stereo S048) has also single leaky intermediate strip, which is identified by HPK.

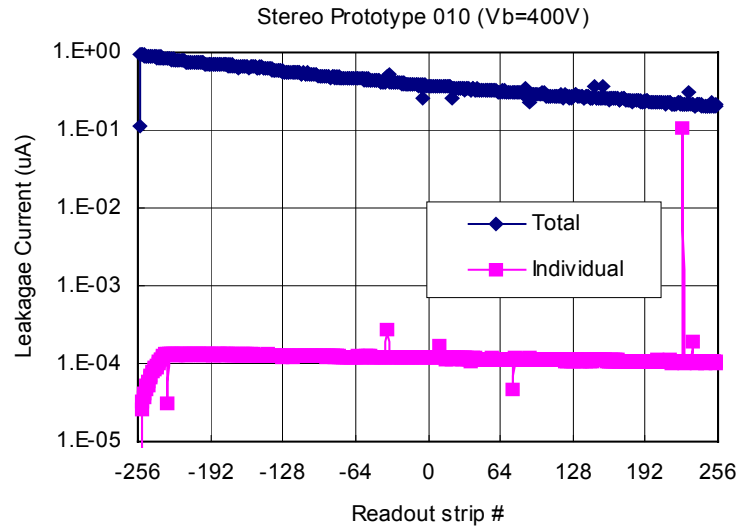


Fig. 5 DC scan (stereo S010) measured at 400V

3.6 Interstrip Resistance

The interstrip resistance is evaluated by measuring the increase/decrease in the strip leakage current when DC voltages ($\pm 1, \pm 0.5 \text{ V}$) are applied to the intermediate strips at neighbor. The four resistance values so obtained are averaged to represent the interstrip resistance. Three axial sensors have been measured. Two distributions are shown in Fig. 6. Although the characteristics look different, the averages are 50-200 $\text{G}\Omega$ and no strip is smaller than $1 \text{ G}\Omega$, our specification. Another sample (Axial A016) showed a distribution very similar to A026 Sensor. A001 was measured right after the delivery (i.e. production) and other two were measured about one month later. The difference could be instrumental, but we suspect that A001 is exceptional “remembering” the process conditions and usual sensors should look like S026 after conditioned. Unfortunately this hypothesis can not be checked, since A001 is irradiated with neutrons.

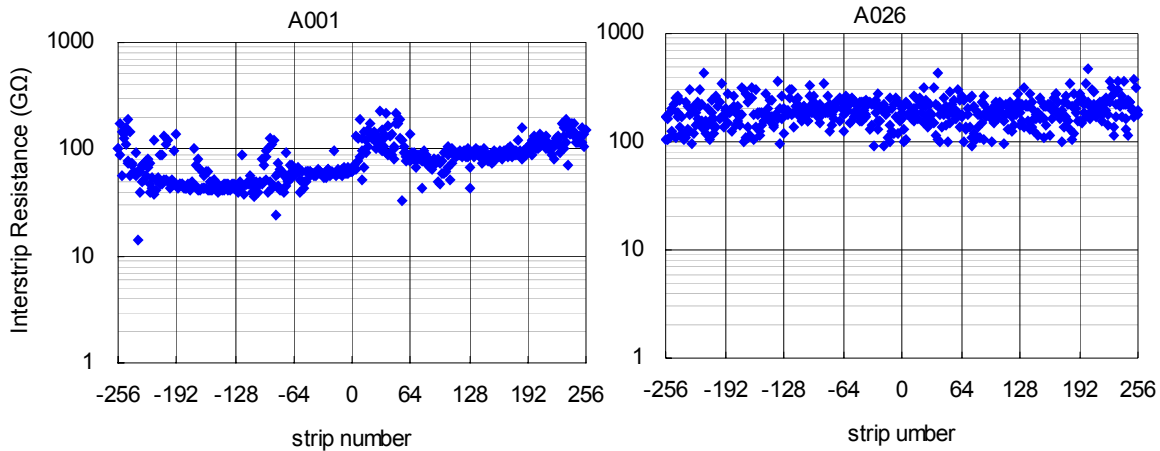


Fig. 6 Interstrip resistance of (left) A001 and (right) A026 Sensors.

3.7 Interstrip Capacitance

The interstrip capacitance is measured by probing neighboring (readout) AC pads with other strip at floating. The bias is set to 200 V and the LCR frequency at 1 MHz. The interstrip capacitance is quite uniform representing the strip length (See Fig 7a). Note that the absolute values are different by 0.3 pF, which should be attributed to the calibration accuracy of our system.

We have measured the interstrip capacitance of in total 9 axial and 2 stereo sensors. Although most of the sensors showed distributions quite similar to those in Fig. 7a, 1 axial and 1 stereo sensors showed irregular values, one pairs for each. An example is given in Fig. 7b. In fact the irregularity for this sensor did not

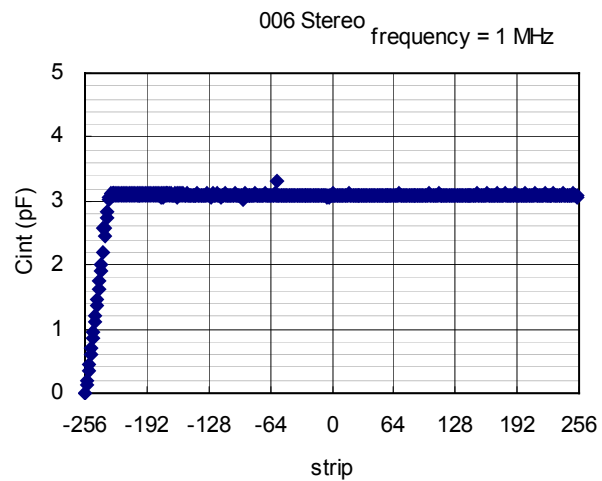


Fig. 7b Interstrip capacitance: Sensor S006 (stereo) with an irregular value.

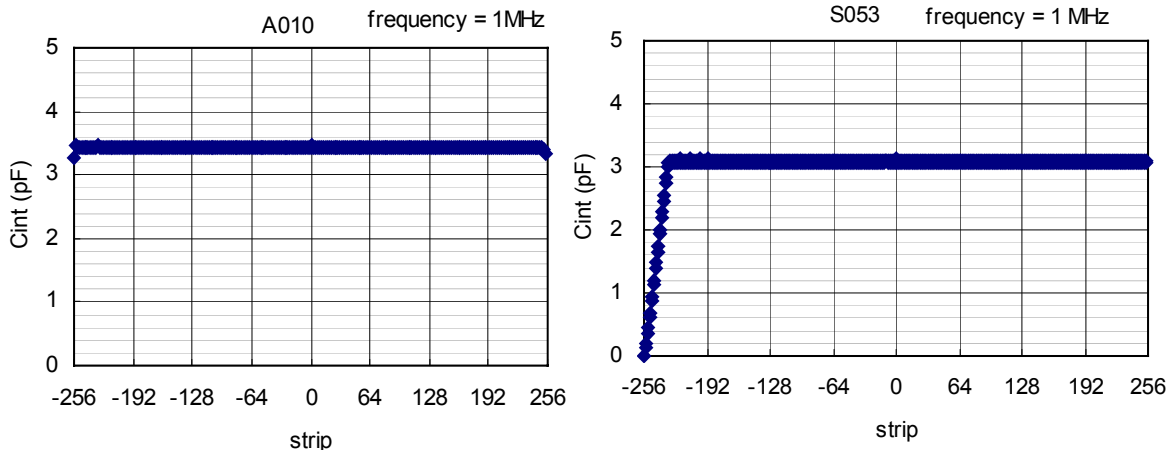


Fig. 7a Interstrip capacitance for (left) axial 010 Sensor and (right) Stereo 053 Sensor.

present at the first measurement, but it appeared. In the time between the probe scratched out the AC pad by miss-operation. Similar thing may have happened to other sensor, and we suspect these irregularities are created during the testing at Tsukuba. There is no other problem found for these strips by visual inspection under microscope.

3.8 Long-term stability test

The stability of leakage current is tested as a part of the electrical characterization. The measurement is still on going, and the results are presented in a separate note.

3.9 Visual Inspections

The delivered sensors have been visually inspected under microscope. Also, faulty strips reported by HPK and found by our scan are inspected more carefully.

The axial sensors are in general clean and we did not recognize major flaws. As described in Section 2, though, the stereo sensors showed visible problems. Figure 8a is a typical picture found for about 1/3 of delivered stereo sensors. They are classified as Class B, since visual inspection does not pass the criteria. Enlarged view (Fig.8a right) shows that the black stains are on the very surface of Al traces. As explained before, these were created when the wafers were taken out manually from the process line, which is not expected to happen in the production. We checked whether there are any correlations between faulty strips and the stains, and between magnitude of stains and shape of I-V curves, but there are no apparent correlations.

A yellow spot shown in Fig. 8b is found only for S010 sensor. Stereo S010 sensor showed micro-discharge, but the contributing strip is not the one in this yellow spot.

From these observations, we conclude that these sensors are good in electrical performance. We classify them as Class B (do not use them, unless delivery becomes a major problem for completion of the project).

Figure 8c shows examples of implant opens both for intermediate strips. The open for A011 sensor is exceptional, and all the other opens look similar to the one found for Axial 010 Sensor (intermediate strip IU125).



Fig. 8a Example of stains observed for stereo sensors. (Right) Enlarged view.

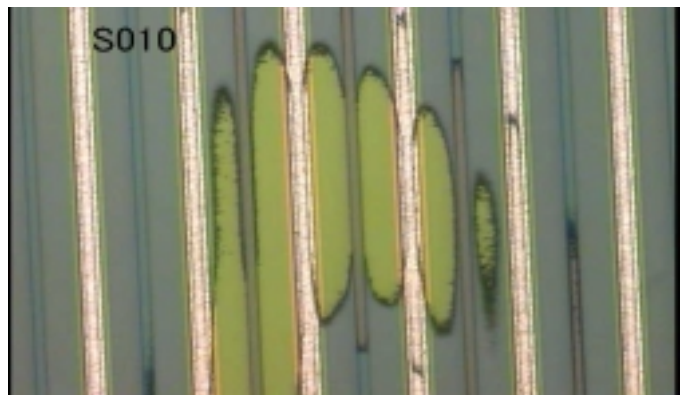


Fig. 8b Yellow spot found for Stereo 010 Sensor.

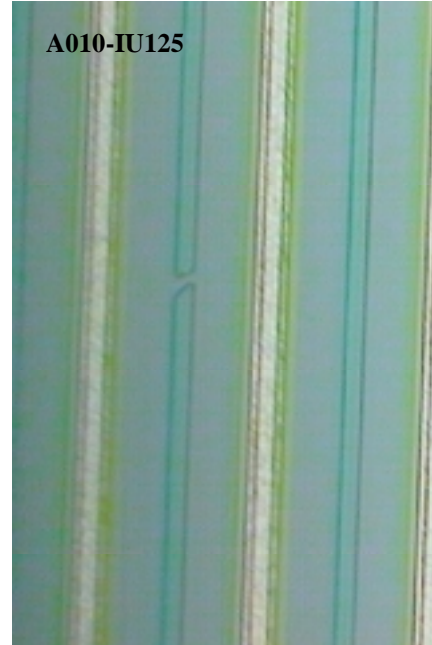
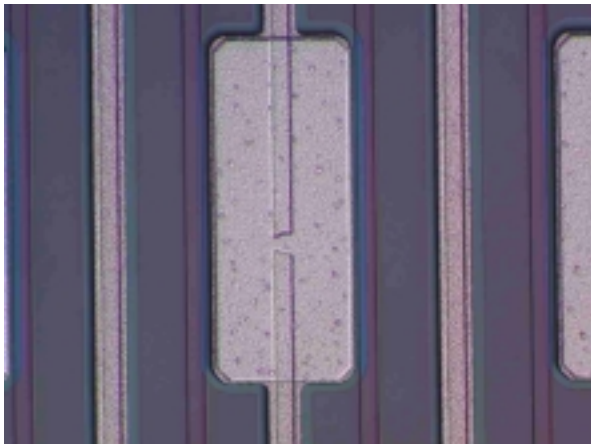


Fig. 8c Examples of implant opens. (Left) Axial 011 Sensor and (Right) Axial 010 Sensor



Some opens are found in the readout implant, one example being shown in Fig. 8d. This is a special case that the break is located underneath the Al bonding pad. Although AC scan at Tsukuba first detected the irregularity of this strip, we failed to find this open under microscope. This sensor was then sent back to HPK for investigation, where this open was identified. This lessons us that very careful inspection is required to find the implant open which is partially hidden by Al electrode on top.

Fig. 8d Readout implant open found underneath the AC pad.

4. Summary of the QA Measurements and Comparison with Manufacturer's Data

4.1 Axial Prototypes

Out of 60 delivered sensors, 18 are studied in detail the characteristics described so far. Sensors with dead channels and worse I-V characteristics are preferentially selected. Table 2 summarizes the dead channels compared between HPK and Tsukuba measurements.

Table 2. Dead channels of axial prototypes compared between HPK and Tsukuba measurements. For disagreements, channels with clear defects are in red.

sensor	HPK	Tsukuba
1		
2		
5		RU62 (Ccp=93pF, R=1.77MΩ, Implant open)
7		RD252 (R=1.1MΩ) RD251 (R=1.1MΩ) trace of small discharge
10	IU244 (Implant open)	IU244 (R=large)
	IU241 (Implant open)	IU241 (R=large)
	IU126 (Implant open)	IU126 (Implant open)
11	IU183 (Implant open)	IU183 (Implant open)
12		RU240 (Ccp=1.07nF, R=2.94MΩ, Icp= 8.1uA)
16		
20		RD231 (167pF, 1.45MΩ, 6uA) RD217 (887pF, 2.63MΩ, 8uA)
21		
23		RD242 (252pF, 3.7MΩ, 8uA), RD241 (149pF, 2.9MΩ, 8uA) RD240 (4860pF, 1.7MΩ, 8.3uA) RD200 (197pF, 3.7MΩ, 8uA) RD194 (155pF, 3.7MΩ, 8uA), RD116 (1920pF, 2.6MΩ, 8uA)
26		
53		
54	ID237, ID240 (Leaky strip)	RD256 (129pF, 1.15MΩ, 8.1uA)
	RD249, RD250 (Leaky strip)	RD249 (120pF, 2.0MΩ, 1.5uA)
		RD248 (3291pF, 1.6MΩ, 8.3uA)
		RD244 (292pF, 3.7MΩ, 8.0uA)
56		
62		
64		
67	ID229, ID230, RD230 (Bad isolation)	RU136 (Ccp=80pF, R=1.6MΩ, implant open)

The reason for the dead is given in the parentheses. In red, we denote that we found new defects and the reason is understood. If we cannot identify the reason for new defects, they are in blue (There is no case for axial sensors).

The two strips (I-U244 and I-U241; “I” refers intermediate strip and “R” readout strip) of Sensor 10 have no obvious opens found under microscope, but the resistance measured between the DC pad and the bias-ring was large. The bias resistor is located other end for the intermediate strips. Probably the joint between the DC pad and implant strip is not fine, which can not be identified by microscope.

None of the leaky strips (Sensor 54) and bad isolation strips (Sensor 67) was identified at Tsukuba. It is quite possible that they disappeared by keeping bias on for a while. Therefore, these disagreements are ignored.

In total 12 punch-throughs are “created” by Tsukuba measurement. After discussion with HPK, it turned out that HPK tested the punch-through by applying a voltage of 100 V for 1/6 sec. Since we apply 100V for 1 sec (or multiple of 1 sec if the measurement is repeated), it is not strange that some punch-throughs are created. HPK should have tested at 120 V, which is the specification and was actually the case for the stereo prototypes. We can ignore these disagreements since we did not see any new punch-through for stereo sensors, as described later.

Sensors 5 and 67 have one implant open for each, which were detected at first by AC scan and then identified by microscope, whereas HPK could not detect them. An explanation is given in Section 4.3 after describing the summary for stereo sensors.

After all, two strips (Sensor 7, RD251 and RD 252) were new and not clearly understood. This sensor (and some other sensors) was sent back to HPK to investigate the problem. According to HPK investigation, small discharge should have happened. The photograph taken by HPK is shown in Fig. 8d. The DC pads of these strips are colored and black discharge traces are visible bridging the two pads.

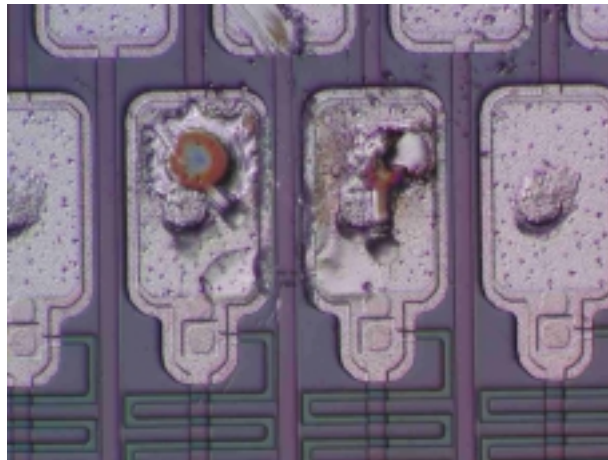


Fig. 8d Photograph around DC pads of RD251 and RD252. Two black traces are visible bridging the two DC pads. (Photo taken by HPK)

4.2 Stereo Prototypes

Out of 53 delivered sensors, 18 sensors are studied in detail on the strip integrity. The comparison is given in Table 3. All the defect strips reported by HPK are identified at Tsukuba. In addition, we found three identified implant opens for readout strips (Sensor 10, RU75; Sensor 23, RU2; Sensor 53, RD24), and one un-identified defective strip (Sensor 13, RD83). There is no punch-through created since HPK tested at 120V.

Table 3. Dead channels of stereo prototypes compared between HPK and Tsukuba measurements. For disagreements, channels with understood defects are in red and others in blue.

sensor	HPK	Tsukuba
6		
7		
10	RU225 (Leaky)	RU225 (leaky)
		RU75 (C=55,R=1.16; implant open)
23		RU2 (C=40,R=0.88; implant open)
24		
47	IU158 (Implant open)	IU158 (Implant open)
65	IU59 (Implant open)	IU59 (R=20M)
66	IU238 (Implant open)	IU238 (implant open)
68	IU21 (Implant open)	IU21 (implant open)
69		
13		RD83 (C=111, R=1.77)
46		
49	IU147 (Implant open)	IU147(R=large)
50		
53	ID7 (Implant open)	ID7 (implant open)
		RD24 (C=90,R=1.6, implant open)
57	ID62 (Implant open)	ID62 (implant open)
63	ID146 (Implant open)	ID146 (implant open)
25	ID230 (Implant open)	ID230 (implant open)

4.3 Implant Opens and Some Technical Difficulties

We have detected five implant opens that were not detected by HPK. These are all readout strips. A possible explanation is sketched in Fig. 9. HPK carries out two kinds of tests, DC and AC tests. In the AC test, HPK injects a step pulse on the AC pad and measures the transient signal shape to detect oxide punch-through (evaluate coupling capacitance) and aluminum strip break/bridge. This procedure is reliable and has been used for many years. In the DC test, HPK applies a DC voltage between the DC pad and bias-ring, and measures the current. This is most sensitive for poly-silicon resistance but also can provide information for the implant open and strip isolation. Since the intermediate strip implant is connected to the bias resistor at far end, the measurement is sensitive to any break in the implant. On the contrary, the system is not sensitive for the readout strip open since the implant is connected to the ground at the probing end. Since we do not request DC pads on other end to avoid openings where hybrids are glued, it is not possible to enhance the sensitivity for readout strip opens. HPK is expecting the AC scan has some sensitivity for the opens locating the near end. The five opens detected by Tsukuba locate about 2 cm, 3 cm, 7cm, 7cm and 8 cm from the probing end¹. We have to conclude that the HPK measurement is barely sensitive for detecting readout implant opens.

There is no reason for the fraction of implant opens being different between intermediate and readout strips. HPK reports 13 opens for the intermediate while we identified 5 opens for the readout. Therefore it is probable that we are still missing some more readout implant opens. Also we should foresee to have some un-identified readout implant opens since our AC scan can be done only for sampled sensors.

Similar difficulties exist for stereo sensors. In our design most of the probed short strips are not read out, but 12 (19 if transceivers are used) strips not starting from the end will be connected to the ASICs. The DC pads for these strips are located at the other end but the nearby bias-ring, which is required for reliable probing, is passivated. Although we could change the mask and open the passivation, probing these extra strips only is another time consuming task, which HPK wants to avoid. It is a reasonable decision not to probe these short strips.

We therefore have to accept some un-identified defective short strips and readout implant opens to exist before connecting to the hybrid. It should be safe to say that if the number of identified defects is small, the number of such un-identified defects should also be small. A good thing is that most of HPK sensors have zero defect! .

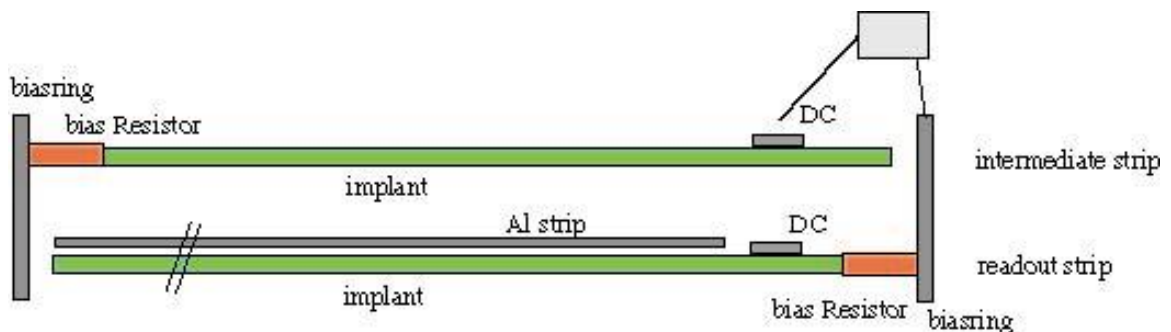


Fig. 9 Illustration of measurement configurations of readout and intermediate implant opens.

¹ HPK re-visited their data if there is any hint for these three strips and also re-measured some of the sensors that have readout implant opens, but failed to identify the defects.

5. Mechanical Precisions

Mechanical precisions of the sensors are measured with Mitutoyo MF-UA measuring microscope. The reproducibility is about 2 μm horizontally and 3 μm vertically. The vertical position is obtained by focusing.

5.1 Wafer thickness

The wafer thickness was measured for 24 sensors at the center of shorter sides. The sensors were placed vertically on the stage under the microscope. The distribution of 48 measurement results is shown in Fig. 10a. The central value is 320 μm with a spread of about 5 μm . Since we used wafers of the same lot, the spread may become wider at production. The precision quoted by HPK is 15 μm .

The thickness difference at the two sides of the same sensor was at maximum 5 μm .

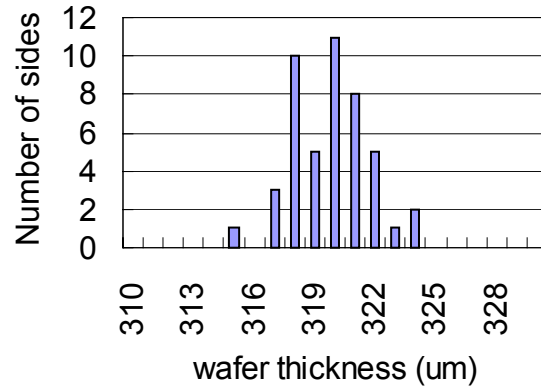


Fig. 10a Wafer thickness distribution

5.2 Edge Cut Precision

The distance between the fiducial mark to the edge was measured at the four corners. The nominal distance is 330 μm . Although no systematic difference between axial and stereo sensors was seen, there are some systematic deviations among the different sides. The right side (shorter hybrid side) tends to be wider than the nominal distance while the left side (shorter probing side) tends to be narrower. Such a difference is smaller for the longer sides. The edge cutting for the present samples is precise to 5 μm , although the quoted precision is 20 μm .

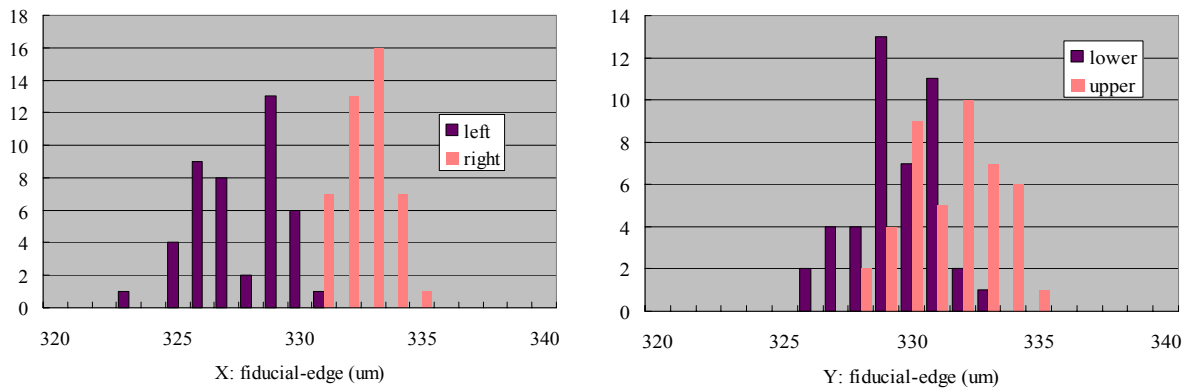


Fig. 10b Distance between the fiducial to the edge.

5.3 Sensor Planarity

The sensors tend to be bowed due to the difference in CTEs between SiO_2 and Si: They are flat at high temperature when processed. The bow is more significant for single-sided sensors than for double-sided sensors.

The general profile is measured on 1 cm grids with a laser system at first. Typical results are given in Fig. 10c, where the three corner data are used to define the reference plane and the deviations to it are plotted. The positive deviations mean that the sensor is bowed with the strip on convex side. The profile is generally universal among the different sensors.

In order to increase the statistics, the height at the sensor center was measured with a microscope together with the heights at the fiducials when the edge cut precision data were taken. The height relative to the fiducial heights is histogrammed in Fig. 10d. The warp is typically 80 to 100 μm for axial sensors, while it is 55 to 90 μm for stereo sensors. The difference could be qualitatively explained by that the stereo sensors are wider than axial sensors.

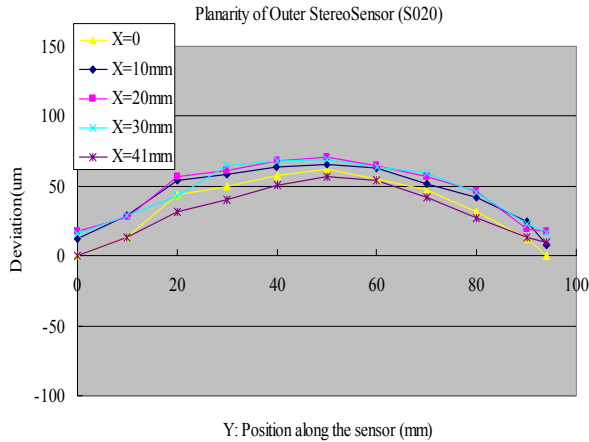


Fig. 10c Typical Z profile of a stereo sensor

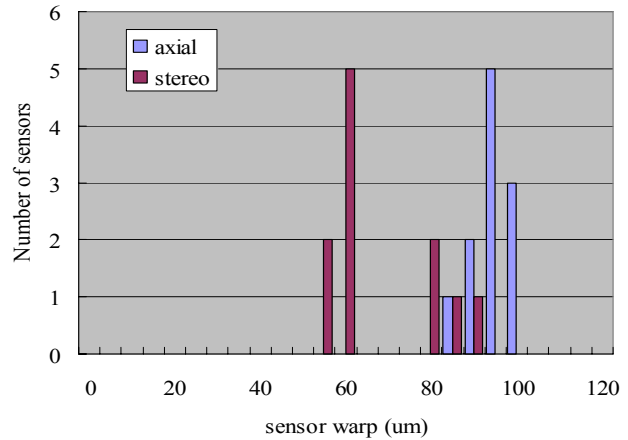


Fig. 10d The deviation in Z at the sensor center

8. Conclusions

We have evaluated the electrical performance of axial and stereo prototypes fabricated by HPK for the SVX2b detector. The prototypes fulfill our specifications. The leakage current is small and most sensors show no breakdown up to 1000V, our specification being 500V. The number of dead channels is quite small. We fully understood the faulty strips reported by HPK. In addition, we found some new faulty strips. We have recognized that HPK test system is not sensitive to detect readout implant opens: We found five new readout implant opens out of in total 36 tested sensors (out of more than 18k strips).

The mechanical precisions, wafer width uniformity, edge cut precision and sensor bowing, were measured. The wafer width and edge cutting are precise to 5 μm , within the specification

Characteristics of irradiated sensors and longer-term stability test results are covered in the separate note (CDF 6287).